A complete map of the ion chemistry of the naphthalene radical cation? DFT and RRKM modeling of a complex potential energy surface

Eduardo A. Solano and Paul M. Mayer

Citation: The Journal of Chemical Physics **143**, 104305 (2015); doi: 10.1063/1.4930000
View online: http://dx.doi.org/10.1063/1.4930000
View Table of Contents: http://scitation.aip.org/content/aip/journal/jcp/143/10?ver=pdfcov
Published by the AIP Publishing

A complete map of the ion chemistry of the naphthalene radical cation? DFT and RRKM modeling of a complex potential energy surface

Eduardo A. Solano[a] and Paul M. Mayer[a,b]
Department of Chemistry and Biomolecular Sciences, University of Ottawa, Ottawa, Ontario K1N 6N5, Canada

(Received 16 June 2015; accepted 21 August 2015; published online 8 September 2015)

The fragmentation mechanisms of the naphthalene molecular ion to $[M–C_4H_2]^{+\bullet}$, $[M–C_2H_2]^{+\bullet}$, $[M–H_2]^{+\bullet}$, and $[M–H^\bullet]^+$ were obtained at the UB3LYP/6-311+G(3df,2p)//UB3LYP/6-31G(d) level of theory and were subsequently used to calculate the microcanonical rate constants, k(E)'s, for all the steps by the Rice-Ramsperger-Kassel-Marcus formalism. The pre-equilibrium and steady state approximations were applied on different regions of the potential energy profiles to obtain the fragmentation k(E)'s and calculate the relative abundances of the ions as a function of energy. These results reproduce acceptably well the imaging photoelectron-photoion coincidence spectra of naphthalene, in the photon-energy range 14.0–18.8 eV that was previously reported by our group. Prior to dissociation, the molecular ion rapidly equilibrates with a set of isomers that includes the *Z*- and *E*-phenylvinylacetylene (PVA) radical cations. The naphthalene ion is the predominant isomer below 10 eV internal energy, with the other isomers remaining at steady state concentrations. Later on, new steady-state intermediates are formed, such as the azulene and 1-phenyl-butatriene radical cations. The naphthalene ion does not eject an H atom directly but eliminates an H_2 molecule in a two-step fragmentation. $H^\bullet$ loss occurs instead from the 1-phenyl-butatriene ion. The PVA ions initiate the ejection of diacetylene (C_4H_2) to yield the benzene radical cation. Acetylene elimination yields the pentalene cation at low energies (where it can account for 45.9%–100.0% of the rate constant of this channel), in a three-step mechanism starting from the azulene ion. However, above 7.6 eV, the major $[M–C_2H_2]^{+\bullet}$ structure is the phenylacetylene cation. © *2015 AIP Publishing LLC*. [http://dx.doi.org/10.1063/1.4930000]

I. INTRODUCTION

Naphthalene is a widespread chemical produced by natural or anthropogenic sources,[1] implied in combustion processes[2–4] which is permanently released into the atmosphere, attracting the attention of the health sciences.[5,6] In the atmosphere, most naphthalene is in the gas phase,[1] and since it absorbs UV radiation,[7] photolysis can be an important transformation,[8] resulting in a complex and not completely understood chemistry. In this context, the gas-phase chemistries of naphthalene, its ions, radicals, and decomposition products are important for different fields of knowledge, especially when these species are generated by UV radiation. This is the case of photoelectron-photoion coincidence (PEPICO) spectroscopy, in which a gas-phase molecule is ionized by vacuum-ultraviolet (VUV) photons, and both the photoelectron and the photoion are detected in delayed coincidence.[9] Different mass spectrometry techniques have been used to study the energetics of the decompositions of the radical cation of naphthalene ($[C_{10}H_8]^{+\bullet}$, m/z 128) and to shed light on the products.[10–12] Both collision-induced dissociation (CID) mass spectrometry at high center-of-mass collision energies and iPEPICO (imaging PEPICO) spectroscopy show four fragmentation channels, namely, loss of $H^\bullet$ ($[C_{10}H_7]^+$, m/z 127), H_2 ($[C_{10}H_6]^{+\bullet}$, m/z 126), C_2H_2 ($[C_8H_6]^{+\bullet}$, m/z 102), and C_4H_2 ($[C_6H_6]^{+\bullet}$, m/z 78). Additionally, the fragment ion $[M–H^\bullet]^+$ generates the ions m/z 126, 101, and 77 by both CID and metastable dissociation.[12]

Scheme 1 shows some possible reactions to account for the fragmentation of the molecular ion **1**. For the formation of $[M–H^\bullet]^+$, it is usually assumed to be a direct C–H bond dissociation, either from the α- or β-positions of **1** (**F4a**, **F4b**), with a critical energy E_0 ranging from 4.20 to 4.48 eV.[10–12] A small energy difference of 0.05 eV between **F4a** and **F4b** has been calculated.[13] Similarly, ion $[C_{10}H_6]^{+\bullet}$ (**F3a** in Scheme 1) could be generated by H_2 loss from **1**,[12–14] with a critical energy of 4.72 eV,[12] but $H^\bullet$ loss from the fragment ion $[C_{10}H_7]^+$ is also possible.[12,14] On the other hand, ion **1** has to rearrange to produce $[M–C_2H_2]^{+\bullet}$ and $[M–C_4H_2]^{+\bullet}$. The two main structures usually considered for the fragment ion $[C_8H_6]^{+\bullet}$ are the benzocyclobutadiene[15] (**F2a**) and phenylacetylene[11] (**F2b**) cations, generated by multistep isomerizations (**1** →→ **12**, **1** →→ **10**) followed by dissociations (Scheme 1).[13] Schroeder and co-workers have provided some experimental evidence in favor of **F2a**.[15] The pentalene cation (**F2c**) has been reported as a possible product, but coming from the isomeric ion **11** (the azulene molecular ion),[13] an ion that should be taken

[a]E. A. Solano and P. M. Mayer contributed equally to this work.
[b]Author to whom correspondence should be addressed. Electronic mail: pmmayer@uottawa.ca. Telephone: 1-613-562-5800 ext. 5769. FAX: 1-613-562-5170.

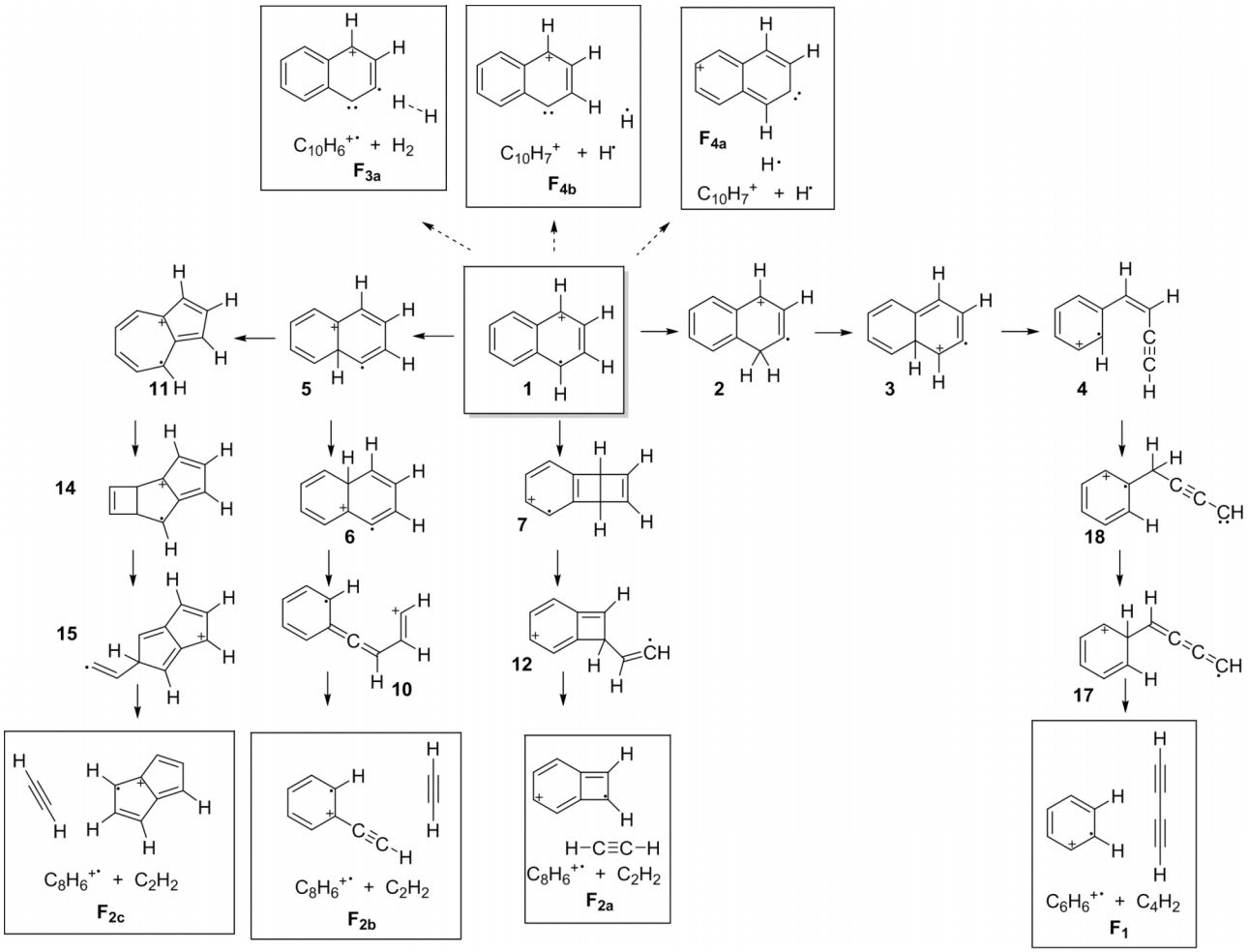

SCHEME 1. Unimolecular decompositions of the naphthalene molecular ion **1**.[11,12] Multiple arrows represent multiple elementary steps. Dashed arrows show those steps for which no first-order saddle point transition state has been reported.

into account because the photoionization mass spectra at 20.58 eV of **1** and **11** are almost identical.[13] Dyakov and co-workers[13] have obtained an impressively complete collection of potential energy profiles for the photodissociations of the molecular ions of naphthalene and azulene, calculated at the G3(MP2,CC)//B3LYP level of theory. According to this modeling, a photoexcited azulene cation can isomerize to a naphthalene cation (Scheme 1 shows the minimum-energy reaction pathway from **1** to **11**).[13]

In the present work, a reaction mechanism is obtained at the UB3LYP/6-311+G(3df,2p)//UB3LYP/6-31G(d) level of theory to produce the fragment ions **F1**, **F2a**, **F2b-c**, **F3a**, **F4a**, and **F4b** (and a new linear isomer $[M–H^{\bullet}]^+$, **F4c**) from **1**, on the basis of the energy profiles of Dyakov and co-workers.[13] The Rice-Ramsperger-Kassel-Marcus (RRKM) rate coefficients for all the steps are then calculated, and an approximate kinetic treatment of the rate equations is applied to simplify the kinetic schemes and obtain general unimolecular rate constants. Finally, the global rate constants are used to calculate the theoretical breakdown graph (a plot of relative abundances of the ions as a function of photon energy) of naphthalene. The results are compared to the iPEPICO data previously reported for this ion by our lab.

II. COMPUTATIONAL DETAILS

A. Potential energy surfaces (PES's)

Density functional theory (DFT) calculations were carried out by using the Gaussian 09 package.[16] The geometric parameters for all ions and transition states (and for the neutral molecule) were completely optimized at the UB3LYP/6-31G(d) level. Each stationary structure was characterized as a minimum or a saddle point of first order by frequency calculations, which were also used to obtain the zero-point vibrational energies (ZPVEs) and the vibrational modes. Intrinsic reaction coordinate calculations[17] were carried out in all cases to verify that the localized transition state structures connect with the corresponding minimum stationary points associated with reactants and products. To obtain more reliable energy results, single-point calculations were performed at the UB3LYP/6-311+G(3df,2p) level using the UB3LYP/6-31G(d) equilibrium geometries. The UB3LYP/6-31G(d) harmonic frequencies were scaled by 0.9806[18] to calculate the ZPVEs and by 0.9614[18] to be used in the RRKM calculations. Ion **1** was selected as the reference zero-point energy of the potential-energy-surface profiles, $E_{gs(1)} = 0.00$ eV (note that E_{gs} is used here to indicate the ground-state energy of the species).

B. Density of states, sum of states, and RRKM calculations

All the calculations implied in the modeling of rate coefficients and vibrational states were performed by running Python 3.1 scripts, especially written to implement the equations of this work. The density of states of every ion s, $\rho_s(E)$, and the sum of states of every transition state i, $N_i^{\ddagger}(E)$, were calculated from the UB3LYP/6-31G(d) vibrational frequencies by the direct-count algorithm of Beyer-Swinehart,[19–21] using bins of 0.12 meV ($\approx$1.0 cm^{-1}) from 0 to 30 eV of vibrational energy excess (see supplementary material for the Python code).[29] The low frequency internal torsional modes were treated as vibrations. Most of the species in the schemes are fairly rigid molecules that do not incorporate hindered internal rotors (see supplementary material for a comparison of $k(E)$ calculated with and without a hindered internal rotor for one of the ring-opened structures in the fragmentation scheme).[29] The energy scale was the same as that of the reaction profiles, with ion **1** as the zero-point reference; thus, the $\rho_s(E)$'s were counted from the ground state (gs) of the corresponding ion s, at $E = E_{\mathrm{gs}(s)}$ above the reference level $E_{\mathrm{gs}(1)}$. For instance, ρ_2 starts at $E_{\mathrm{gs}(2)} = 2.11$ eV = 17 018 cm^{-1} and ρ_{4E} at $E_{\mathrm{gs}(4E)} = 2.23$ eV = 17 986 cm^{-1}, which means that $\rho_s(E) = 0$ cm for energies $E < E_{\mathrm{gs}(s)}$. Similarly, the $N_i^{\ddagger}(E)$'s were counted from the ground state of the corresponding transition state i at $E = E_{\mathrm{gs},i}^{\ddagger}$ above the reference level (note that $E_{\mathrm{gs},i}^{\ddagger}$ is the ground-state energy of the transition state with respect to that of ion **1**). The RRKM rate constant for every individual step, $k_i(E)$, was calculated by using Eq. (1)[20,21] from the density of states of the parent ion s at energy E, $\rho_s(E)$, and the sum-of-states of the transition state i, $N_i^{\ddagger}(E)$. In addition, σ_i is the reaction degeneracy and was chosen to represent the number of degenerate pathways for a given reaction,[20] while h is Planck's constant,

$$k_i(E) = \frac{\sigma_i N_i^{\ddagger}(E)}{h\rho_s(E)}. \quad (1)$$

The magnitudes of the k_i's at the same energy interval were used as the criterion to compare elementary steps and establish if they were reversible and to decide which species could be treated as being either in a steady state or an equilibrium.

C. Kinetic modeling

The reaction mechanism network was reduced to the one shown in Scheme 2(a), where **M** and the $\mathbf{I}_\alpha$'s represent mixtures of isomers of the molecular ion, differing by their lifetimes and concentrations. The components of **M** were assumed to survive long enough to stay at equilibrium with one another; this is the *equilibrated parent-ion mixture* ($[\mathbf{M}] = [s_{\mathrm{eq},1}] + [s_{\mathrm{eq},2}] + \cdots + [s_{\mathrm{eq},k}]$). In contrast, the components of a given $\mathbf{I}_\alpha$ do not have to be at equilibrium, they constitute a *steady-state intermediate mixture* ($[\mathbf{I}_\alpha] = [s_{\mathrm{in},1}] + [s_{\mathrm{in},2}] + \cdots + [s_{\mathrm{in},k}]$). [**M**] was considered as the concentration that defines the parent ion abundances observed in the mass spectra (I_M), and [$\mathbf{I}_\alpha$] as being at a steady state as a

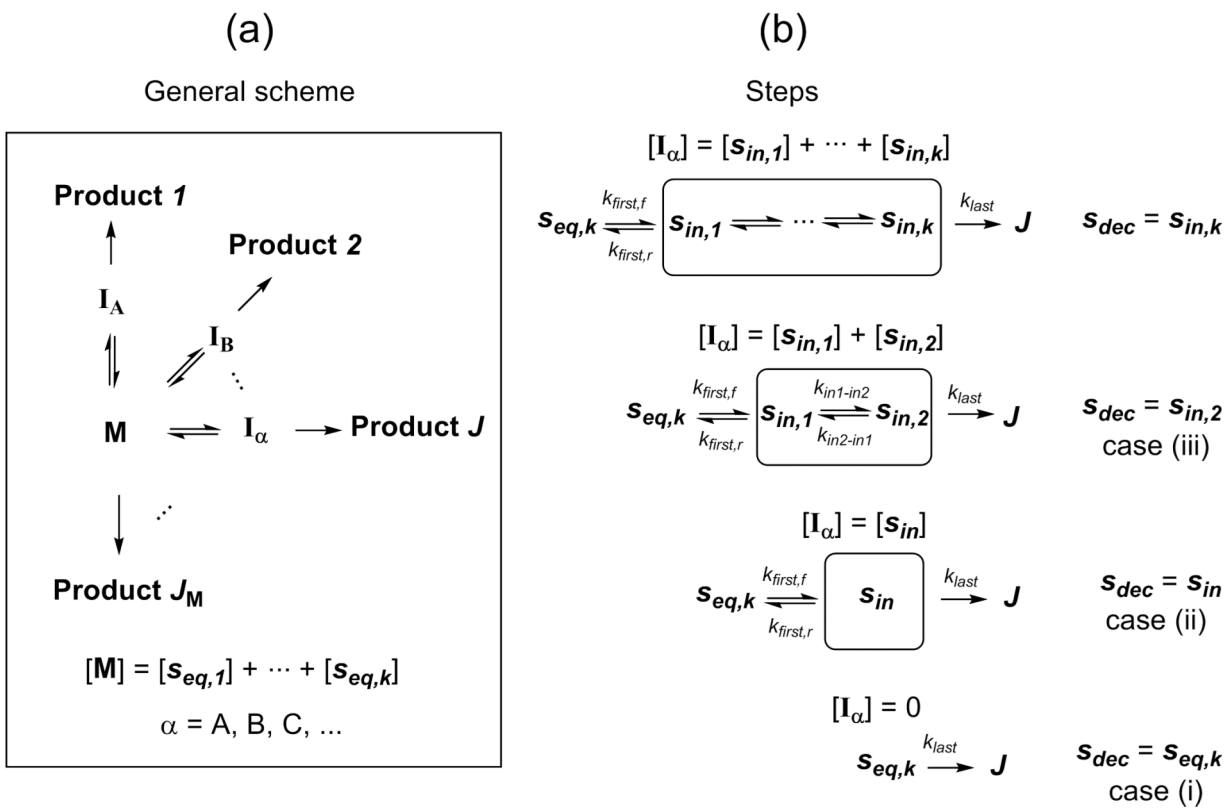

SCHEME 2. (a) General kinetic scheme for the decomposition of the parent ions **M** into multiple channels J with or without a steady-state intermediate $\mathbf{I}_\alpha$. The parent ions consist of an equilibrated mixture of isomers. (b) Generalization of the elementary steps that can lead to a product (the intermediates can be an individual species or a mixture of them). The decomposing species $s_{\mathbf{dec}}$ is an isomeric ion present in either the mixture **M** (case (i)) or $\mathbf{I}_\alpha$ (cases (ii) and (iii)).

whole (thereby not contributing to the signal of the parent ion, I_M).

The fragmentation that gives rise to the ion $\boldsymbol{J}$ is governed by

$$\frac{d[\boldsymbol{J}]}{dt} = k_J[\mathbf{M}], \tag{2}$$

where the observed microcanonical rate constant k_J was calculated using

$$k_J = c_J \frac{\sigma_{\text{last}} N^{\ddagger}_{\text{last}}}{h\rho_M}, \tag{3}$$

where $\rho_M = \rho_{s_{\text{eq},1}} + \cdots + \rho_{s_{\text{eq},k}}$ is the *total* density of states of the species of mixture **M**, and $N^{\ddagger}_{\text{last}}$ is the sum-of-states of the transition state for the last step $\boldsymbol{s_{\text{dec}}} \rightarrow \boldsymbol{J}$ in the pathway (Scheme 2(b)) considered as the dissociation (with a reaction degeneracy σ_{last}). This step was typically the dissociation, except for the case of $\mathbf{I}_E$, where an additional rate-controlling step approximation was applied. Equation (3) requires the calculation of the energy-dependent coefficient c_J. c_J acts as the probability that the system reacts with a rate constant k_J. $c_J = 1$ indicates that the parent ion (**M**) decomposition takes place via some species equilibrated with the original molecular ion (**1**). It can also mean that $N^{\ddagger}_{\text{last}} \ll N^{\ddagger}_{\text{first}}$, that is, the reaction proceeds through some steady-state intermediate in which the rate-controlling (slow) step is the last one (k_{last} in Scheme 2). In contrast, $N^{\ddagger}_{\text{last}} \gg N^{\ddagger}_{\text{first}}$ yields a very small value of c_J, indicating that the reaction is controlled by the first step, that is, the one to yield the intermediate $\mathbf{I}_{\boldsymbol{\alpha}}$. For some more competitive situations with $N^{\ddagger}_{\text{last}} = N^{\ddagger}_{\text{first}}$, $c_J = 0.50$.

To determine c_J, differential rate equations were set up for the potential energy profiles, with the complexity being reduced by using either the pre-equilibrium or the steady-state approximations.[22] The Mathematica package,[23] version 8.0, was used to solve the resulting simultaneous algebraic equations and find expressions for the intermediate concentrations. This is the way Eqs. (4)–(6) were obtained. Equation (4) was used for the "direct" decompositions of **M** (case (i) in Scheme 2(b), $\boldsymbol{J}_{\mathbf{M}}$ in Scheme 2(a)) since dissociation is controlled by a single transition state, while Eqs. (5) and (6) were used for decompositions through intermediates composed of one (case (ii)) and two species (case (iii)), respectively. Finally, the total decay rate of **M**, k, (Eq. (7)) was calculated as the sum of the k_J's for every channel J (Eq. (8)),

$$c_J = 1, \text{ case (i)}, \tag{4}$$

$$c_J = \frac{\sigma_{\text{first}} N^{\ddagger}_{\text{first}}}{\sigma_{\text{first}} N^{\ddagger}_{\text{first}} + \sigma_{\text{last}} N^{\ddagger}_{\text{last}}}, \text{ case (ii)}, \tag{5}$$

$$c_J = \frac{\sigma_{\text{first}} N^{\ddagger}_{\text{first}} \cdot \sigma_{\text{in1-in2}} N^{\ddagger}_{\text{in1-in2}}}{\sigma_{\text{first}} N^{\ddagger}_{\text{first}} \cdot \sigma_{\text{in1-in2}} N^{\ddagger}_{\text{in1-in2}} + \sigma_{\text{first}} N^{\ddagger}_{\text{first}} \cdot \sigma_{\text{last}} N^{\ddagger}_{\text{last}} + \sigma_{\text{in1-in2}} N^{\ddagger}_{\text{in1-in2}} \cdot \sigma_{\text{last}} N^{\ddagger}_{\text{last}}}, \text{ case (iii)}, \tag{6}$$

$$\frac{d[\mathbf{M}]}{dt} = -k[\mathbf{M}], \tag{7}$$

$$k = \sum_J k_J. \tag{8}$$

D. Breakdown graph modeling

The breakdown graph was modeled by the minimal-PEPICO program.[9] This program uses the assumption that the internal energies E of the parent ions obey a thermal distribution inherited from the neutral molecule at a constant temperature T (the reported experimental temperature[12] is $T = 298$ K), given by Eq. (9).[9,20] The density of states ρ_{mol} in Eq. (9) is calculated from the frequencies of the neutral molecule in this program, rather than those of the parent ion (the frequencies were scaled by 0.9614). The distribution function is characterized by a given amount of internal energy ($h\nu - IE_{\text{ad}}$) (Eq. (10)), transferred by a VUV photon of frequency ν to the ion during the photoionization of the corresponding neutral whose ionization potential is IE_{ad} ($h\nu \geq IE_{\text{ad}}$). The IE_{ad} value[24] used here was 8.1442 eV,

$$p_M(E, h\nu) = \frac{\rho_{\text{mol}}(E') \cdot \mathrm{e}^{-E'/RT}}{\int_0^{\infty} \rho_{\text{mol}}(E') \cdot \mathrm{e}^{-E'/RT} \cdot dE'}, \tag{9}$$

where

$$E' = E - (h\nu - IE_{\text{ad}}). \tag{10}$$

The theoretical fractional relative abundances of parent and fragment ions, I_M/I_{tot} and I_J/I_{tot}, were calculated by Eqs. (11) and (12),[9,25,26] in which $\tau_{\max}$ is the maximum flight time within which an ion has to dissociate to be recorded as a fragment ion,

$$\frac{I_M}{I_{\text{tot}}}(E, h\nu) = \int_0^{\infty} p_M(E, h\nu) \cdot \mathrm{e}^{-k(E)\cdot\tau_{\max}} \cdot dE, \tag{11}$$

$$\frac{I_J}{I_{\text{tot}}}(E, h\nu) = \int_0^{\infty} p_M(E, h\nu) \cdot \frac{k_J(E)}{k(E)} \left[1 - \mathrm{e}^{-k(E)\cdot\tau_{\max}}\right] dE, \tag{12}$$

$k_J(E)$ is the dissociation rate constant for the channel J (Eq. (3)), and $k(E)$ is the total unimolecular decay rate constant of **M** (Eq. (8)). For this purpose, minimal-PEPICO requires the sum-of-states of every channel, $N_J = c_J \sigma_{\text{last}} N^{\ddagger}_{\text{last}}$ (Eq. (3)), and the density of states of the parent ions, ρ_M, as entries. The experimental breakdown graph was taken from Ref. 12.

III. RESULTS AND DISCUSSION

A. Origin of the kinetic approach

The fragmentation rate to yield $\boldsymbol{J}$ is defined by the species that directly generates it, that is, $d[\boldsymbol{J}]/dt = k_J[\mathbf{M}] = k_{\text{last}}[\boldsymbol{s_{\text{dec}}}]$. Using the definition of k_{last} in terms of the

corresponding sum and density of states (Eq. (1)), this rate equation becomes

$$k_J = \frac{[s_{\mathbf{dec}}]}{[\mathbf{M}]} \frac{\sigma_{\text{last}} N^{\ddagger}_{\text{last}}}{h \rho_{s_{\text{dec}}}}. \tag{13}$$

The decomposing species $s_{\mathbf{dec}}$ is an isomeric ion present in one of the mixtures **M** or $\mathbf{I}_\alpha$. If $s_{\mathbf{dec}}$ takes part of the original parent-ion mixture **M**, $[s_{\mathbf{dec}}] = [s_{\mathbf{eq,k}}]$ (Scheme 2(b), Eqs. (14) and (15)),

$$[s_{\mathbf{dec}}] = k_{\text{dec}} [s_{\mathbf{eq,k}}], \tag{14}$$

$$k_{\text{dec}} = 1, \text{ case (i)}. \tag{15}$$

When $s_{\mathbf{dec}}$ belongs to the intermediate $\mathbf{I}_\alpha$, $[s_{\mathbf{dec}}]$ can also be expressed in terms of some component of **M**, $[s_{\mathbf{eq,k}}]$. By applying the steady state approximation on all the members of $[\mathbf{I}_\alpha]$, $[s_{\mathbf{dec}}]$ turns out to be a product of $[s_{\mathbf{eq,k}}]$ by a function k_{dec} (Eq. (14)), where k_{dec} is a relationship among elementary rate constants (Eqs. (16) and (17)). Equations (16) and (17) describe the decompositions through intermediates $\mathbf{I}_\alpha$ composed of one or two species, respectively,

$$k_{\text{dec}} = \frac{k_{\text{first,f}}}{k_{\text{first,r}} + k_{\text{last}}}, \text{ case (ii)}, \tag{16}$$

$$k_{\text{dec}} = \frac{k_{\text{first,f}} \cdot k_{\text{in1-in2}}}{k_{\text{first,r}} \cdot k_{\text{in2-in1}} + k_{\text{first,r}} \cdot k_{\text{last}} + k_{\text{in1-in2}} \cdot k_{\text{last}}}, \text{ case (iii)}, \tag{17}$$

where the subscripts "f" and "r" refer to the forward and reverse reactions and "in1" and "in2" refer to the intermediate ions in the pathway, Scheme 2(b).

Equations (16) and (17) can be rewritten in terms of the sums and densities of states of the corresponding steps according to Eq. (1), yielding Eq. (18), where c_J had already been defined in Eqs. (4)–(6). Substituting Eq. (18) into Eq. (14) and, then using the resulting $[s_{\mathbf{dec}}]$ in Eq. (13), yields the k_J of

$$k_{\text{dec}} = \frac{\rho_{s_{\text{dec}}}}{\rho_{s_{\text{eq,k}}}} c_J, \tag{18}$$

$$k_J = c_J \frac{[s_{\mathbf{eq,k}}]}{[\mathbf{M}]} \frac{\sigma_{\text{last}} N^{\ddagger}_{\text{last}}}{h \rho_{s_{\text{eq,k}}}}. \tag{19}$$

Finally, according to the current modeling, for the equilibrated mixture defined in Eq. (20), the relative concentrations of the species that take part in it, $[s_{\mathbf{eq,k}}] / [\mathbf{M}]$, are given by Eq. (21), where $\rho_{s_{\text{eq,k}}}$ is the density of states of the species $s_{\mathbf{eq,k}}$, and ρ_M is the *total density of states*, defined in Eq. (22) as the sum of densities of states of all the species involved in the equilibrium. The substitution of Eq. (21) into Eq. (19) yields the resulting k_J shown in Eq. (3),

$$[\mathbf{M}] = \sum_k [s_{\mathbf{eq,k}}], \tag{20}$$

$$\frac{[s_{\mathbf{eq,k}}]}{[\mathbf{M}]} = \frac{\rho_{s_{\text{eq,k}}}}{\rho_M}, \tag{21}$$

$$\rho_M \equiv \sum_k \rho_{s_{\text{eq,k}}}. \tag{22}$$

B. DFT mechanism

Scheme 3 shows the final version of the DFT reaction mechanisms for the unimolecular decomposition of the naphthalene molecular ion, **1**. The central box contains isomeric structures with ground state energies up to 3.57 eV above the ground state of **1** (**11** is an exception). The transition states in this region do not exceed 3.88 eV above the ground state of **1**. More energetically demanding processes are allocated in the side "branches." The final outcome in every branch is a fragment ion, labeled by using the letter F, **F1**–**F4** (an additional lowercase letter is added for isomeric fragment ions, e.g., **F4a**, **F4b**, and **F4c**). Branches A and C–E contain non-covalent dissociating complexes, **C1**–**C4**, with dissociation energies between 0.07 and 0.52 eV (7–50 kJ mol^{-1}). As expected, the complex dissociation is harder for bigger neutrals, so that the interaction energy between diacetylene and the benzene radical cation in **C1** (branch A) is the strongest one at 0.52 eV, whereas the complex acetylene/benzocyclobutadiene cation **C2** (branch D) requires just 0.10 eV to dissociate. Actually, complexes for $[M–H_2]^{+\bullet}$ and $[M–H^\bullet]^+$ can also be found, but since their dissociations do not require any appreciable amount of energy, they were not considered. According to the energy barriers for **C**1 → **17** (0.13 eV) and **C1** → $\boldsymbol{F_1}$ (0.52 eV), complex **C1** (branch A) could even be formed in a reversible way, but its formation was considered as irreversible for simplicity. A similar situation occurs for complex **C3** in branch C. A special issue comes out in complex **C3**, since the transition state by which it is formed lies 0.03 eV below it (this situation stays the same even when just electronic energies are considered with no addition of vibrational energy). This suggests that there must be an alternative arrangement of the complex with a lower ground state. Branch A leads to $[M–C_4H_2]^{+\bullet}$, branch B produces an H atom ejection from the isomeric species 1-phenylbutatriene ion (**16**), and branches C–E end up with acetylene loss. Additionally, there are direct decompositions of the species of the central box for $H^\bullet$ and H_2 losses (**F4a**, **F4b**, and **F3a**).

Branches C–E represent three different mechanisms to lose acetylene, producing the benzocyclobutadiene (**F2a**), phenylacetylene (**F2b**), or pentalene (**F2c**) ions, with the order of products energies being **F2c** (4.09 eV) < **F2b** (4.55 eV) < **F2a** (4.58 eV). In the present modeling, the reaction rates at which the complexes **C1**–**C4** are formed give the fragmentation rates, that is, $d[\mathbf{F_1}]/dt = k_{22}[\mathbf{17}]$, $d[\mathbf{F_{2a}}]/dt = k_{14}[\mathbf{12}]$, $d[\mathbf{F_{2b}}]/dt = k_{16}[\mathbf{10}]$, and $d[\mathbf{F_{2c}}]/dt = k_{20}[\mathbf{15}]$. In addition, for the H atom loss, $d[\mathbf{F_{4a}}]/dt + d[\mathbf{F_{4b}}]/dt = (k_{26} + k_{27})[\mathbf{1}] + k_{24}[\mathbf{6}] + k_{25}[\mathbf{3}]$ and $d[\mathbf{F_{4c}}]/dt = k_{11}[\mathbf{16}]$, and for the H_2 loss $d[\mathbf{F_{3a}}]/dt = k_{23}[\mathbf{8}]$. An additional approximation of rate-controlling step is done on $d[\mathbf{F_{2c}}]/dt$ later.

C. Isomerization of the molecular ion before fragmentation

Ion **1** can readily suffer sequential 1,2-hydrogen shifts, **1** → **2** → **3**, **1** → **5** → **6**, and **1** → **8**, or a ring rearrangement to yield **7**. Additionally, a ring opening can take place from the isomeric structure **3** to yield the *Z*-phenylvinylacetylene

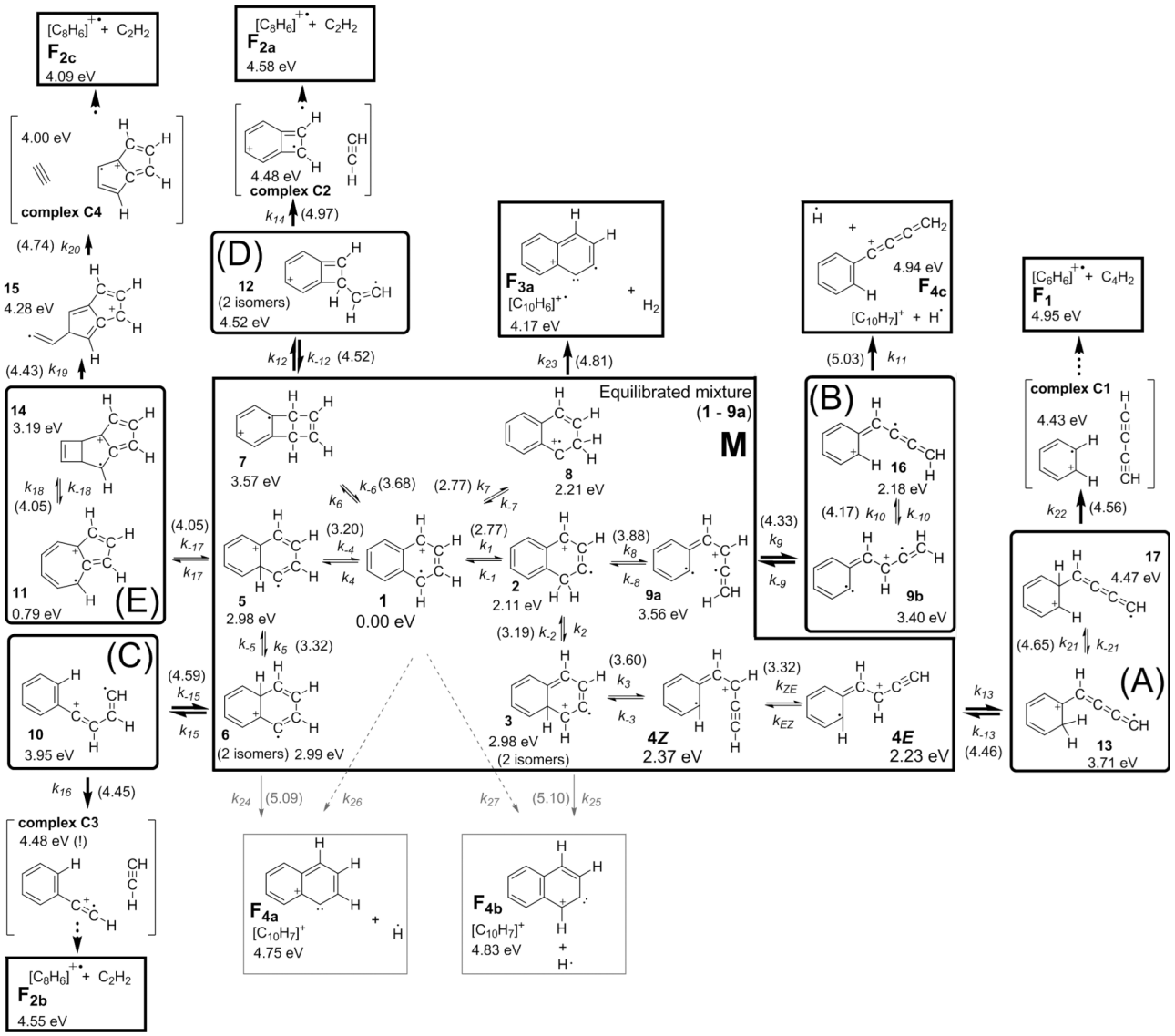

SCHEME 3. Isomerization and dissociation pathways of the naphthalene molecular ion obtained from the UB3LYP/6-311+G(3df,2p)//UB3LYP/6-31G(d) calculations. Calculated relative energies in eV are given for stable species and in parentheses near the corresponding arrows for the transition states. Dashed arrows indicate the steps with no first-order saddle point connecting reactant and products (k_{26} and k_{27} were calculated by removing a frequency from **1**, corresponding to the reaction coordinate). Structures **C1**–**C4** are non-covalent complexes.

(PVA) ion, **4*Z*** (though a similar reaction could happen from **6**, it requires a much higher kinetic barrier, 0.62 eV for **3** → **4*Z*** vs 1.60 eV for **6** → **10**). As soon as it is formed, **4*Z*** stabilizes by a *cis-trans* isomerization (to **4*E***). A more demanding process, but still included in the central region, is the ring opening reaction **2** → **9*a***. The steps in the central box of Scheme 3 have relatively lower kinetic barriers and higher RRKM rate constants with respect to the reactions that turn these species into others outside this box. The rate coefficients for some elementary steps are shown in Fig. 1. Isomerizations of **1**, through 1,2-H shifts (k_1, k_4, and k_7 in Fig. 1(a)) or a ring rearrangement (k_6), are much faster than direct C–H bond dissociations (k_{26} and k_{27}). Actually, there must be some fast H-scrambling before any fragmentation takes place, as can be seen in Figs. 1(b) and 1(c), where the ring expansion **5** → **11** (Fig. 1(b)), ring opening **6** → **10**, and C–H bond dissociation **6** → $\mathbf{F_{4a}} + H^{\bullet}$ (Fig. 1(c)) turn out to be much slower than the corresponding 1,2-H shifts (**5** → **1**, **5** → **6**, and **6** → **5**) in a wide energy range, that is, $k_{17} \ll k_{-4}$, k_5, and k_{15} and $k_{24} \ll k_{-5}$. The ring opening **3** → **4*Z*** (k_3 in Fig. 1(d)) was included in the central region because it is considerably faster than the dissociation **3** → $\mathbf{F_{4b}} + H^{\bullet}$ (k_{25}). Even the azulene ion (**11**), which is the species with the second lowest ground-state energy (0.79 eV, Scheme 3), is harder to be formed from **5** (k_{17} in Fig. 1(b)) compared to other reactions from **5**, and therefore, it was taken as not part of the pre-equilibrium of precursor structures and left out of central box. This way, in a wide range of internal energies, the forward and reverse rate coefficients of the steps of the species in this region are much larger than all others (Fig. 1), and, according to the pre-equilibrium approximation,[22] it might be assumed that the corresponding isomeric structures (**1** – **9*a***) are practically in equilibrium.

According to this approximation, the slowness of the steps pointing to the outside of the equilibrated mixture region gives **1** – **9*a*** enough time to essentially reach an equilibrium state,[22]

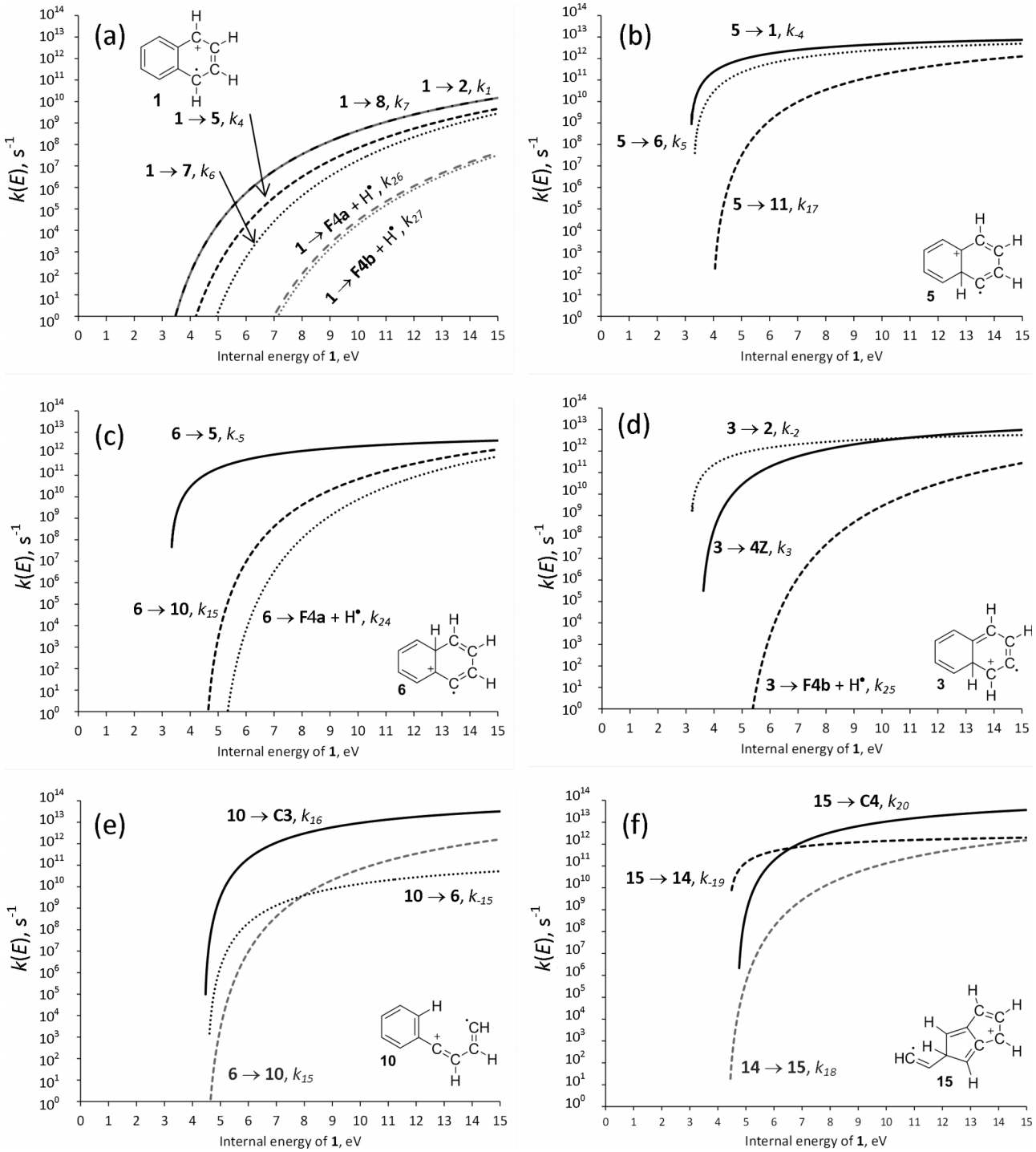

FIG. 1. Microcanonical rate coefficients $k_i(E)$ (Eq. (1)) for some selected individual reaction steps of Scheme 3 vs internal energy above the ground-state level of ion **1**. $\sigma_i = 1$ was used in every case.

that is, $[\mathbf{1}] = [\mathbf{1}]_{eq}$, $[\mathbf{2}] = [\mathbf{2}]_{eq}$, and so on. This way, the ratios $[\mathbf{2}]/[\mathbf{1}]$, $[\mathbf{3}]/[\mathbf{2}]$, etc., can be considered as microcanonical equilibrium constants over the energy range in which the pre-equilibrium is maintained. The equilibrium constants can be calculated either from the density of states of the ions **1** – **9*a***[22] (e.g., $K_1 = \rho_2/\rho_1$ for the step 1) or from the mass action law as the ratio of the corresponding forward to reverse rate constants, e.g., $K_1 = k_1/k_{-1}$. Similar expressions can be written for K_2, K_3, etc. In turn, the ions **1** – **9*a*** can be grouped together and called **M**. The total concentration of these isomeric structures is $[\mathbf{M}] = [\mathbf{1}] + [\mathbf{2}] + [\mathbf{3}] + [\mathbf{4Z}] + [\mathbf{4}\boldsymbol{E}] + [\mathbf{5}] + [\mathbf{6}] + [\mathbf{7}] + [\mathbf{8}] + [\mathbf{9a}]$. This gives rise to a set of ten simultaneous equations with the concentrations of **1** – **9*a*** as the unknowns, and whose solutions have the form of Eq. (21) with $\boldsymbol{s}_{\mathbf{eq,k}} = \mathbf{1}, \mathbf{2}, \ldots, \mathbf{9}\boldsymbol{a}$ and with the total density of states of the mixture being defined by Eq. (22) as $\rho_M = \rho_1 + \cdots + \rho_{9a}$.

The ratio $\rho_{s_{eq,k}}/\rho_M$ in Eq. (21) yields the relative concentration of the corresponding species $\boldsymbol{s}_{\mathbf{eq,k}}$ in **M** (Eq. (21)); thus, the equilibrated mixture is richer in those isomers with the highest densities of states in the unified

energy scale (based on **1**). In addition, since the $\rho_{s_{eq,k}}$'s define the equilibrium constants[22] of the steps, the ratio $\rho_{s_{eq,k}}/\rho_M$ also constitutes a measurement of the relative stability as a function of internal energy, in such a way that, given some energy, the higher the $\rho_{s_{eq,k}}/\rho_M$ the more stable the ion $s_{eq,k}$. In the mechanism of Scheme 3, the densities of states of **1**, **4*Z***, and **4*E*** turn out to be so much higher than those of all other isomers in **M**, in the energy range 0–30 eV, that is, $\rho_M \approx \rho_1 + \rho_{4Z} + \rho_{4E}$. Equation (21) is plotted in Fig. 2 as a function of internal energy of **1** for these three ions, and for **9a** (the fourth in order of abundance) showing that ion **1** is practically pure (>98%) when its energy content is less than 9 eV; then up to 10 eV it accounts for 94% of the concentration of the parent ions and 60% at 14 eV. Concomitantly, the PVA ions **4*Z*** and **4*E*** become increasingly abundant when the excess energy goes up. They appear at appreciable amounts at ~8 eV and added together become a half of the total concentration [**M**] at 15 eV.

In summary, the molecular ion **1** isomerizes very quickly to **4Z** and **4E** via a number of species that stay at low "equilibrium" concentrations over a broad energy range and is thereby undetectable. Nevertheless, these "hidden" isomers define the chemistry behind the mass spectrum of naphthalene, as will be seen later. The ring opening implies a thermodynamic advantage with respect to other isomerizations, because the resulting species exhibit lower vibrational modes that enhance the densities of states. According to the present model, provided that the system overcomes some threshold energy, the naphthalene (**1**) and **4Z**/**4E** molecular ions are completely equilibrated before any fragmentation takes place. Once naphthalene has been ionized, it requires at least an extra energy of 3.60 eV (step **3** → **4*Z***) to start this equilibration. This threshold would be lower if the ionized species were **4Z**/**4E** (for instance, starting from the *Z*-isomer the same step requires just 1.22 eV), which means that these ions are expected to behave like the naphthalene molecular ion in mass spectrometry, but with lower energetic requirements. In principle, the same PES could be used to explain the mass spectra of the **4Z**/**4E** (but there is no quantitative experimental data available to test this hypothesis). On the other hand, although the isomerization that produces the azulene ion (**11**) is slower in most of the energy range shown in Fig. 1(b) (k_{17}), and, consequently, not considered in the equilibrium system, at high energies all these rate constants tend to converge (k_5, k_{-4}, and k_{17} at >~14 eV), which increases the probability that **11** gets involved into the equilibrium. That is why the mass spectra of azulene and naphthalene have been reported as almost identical at high energies.[14]

D. Decomposition of the parent ions

There are five steps by which **M** turns into the side branches A–E (**4*E*** → **13**, **9*a*** → **9*b***, **6** → **10**, **7** → **12**, and **5** → **11**) and the direct fragmentations of **M** that involve C–H bond dissociations to eject either one hydrogen atom (to yield $\mathbf{F_{4a}}$ or $\mathbf{F_{4b}}$) or one hydrogen molecule (**8** → $\mathbf{F_{3a}}$). As mentioned before, all these steps are much slower than the interconversions among the components of **M**. Figure 3 shows some selected molecular models involved in important steps of the mechanism.

First, it should be noted that despite the conventional idea that the naphthalene molecular ion loses hydrogen atoms from the α- or β-positions[12,13] to yield $\mathbf{F_{4a}}$ or $\mathbf{F_{4b}}$, no transition state has been previously reported to account for these reactions, nor does this work succeed in this challenge. To test this assumption, k_{26} and k_{27} were calculated by removing one frequency from **1**, corresponding to the C–H stretching vibrations ν_{43} = 3215 cm^{-1} and ν_{47} = 3239 cm^{-1}, respectively, and using the ground-state energies of the fragment ions $\mathbf{F_{4a}}$ and $\mathbf{F_{4b}}$ (4.75 and 4.83 eV) as the kinetic barriers. These processes were calculated as less likely than the reactions of **1** towards the side branches (k_1, k_4). C–H bond cleavage transition states could be calculated from isomers **3** and **6**, ejecting H• from the central carbon atoms, but these reactions still had considerably higher kinetic barriers (with transition

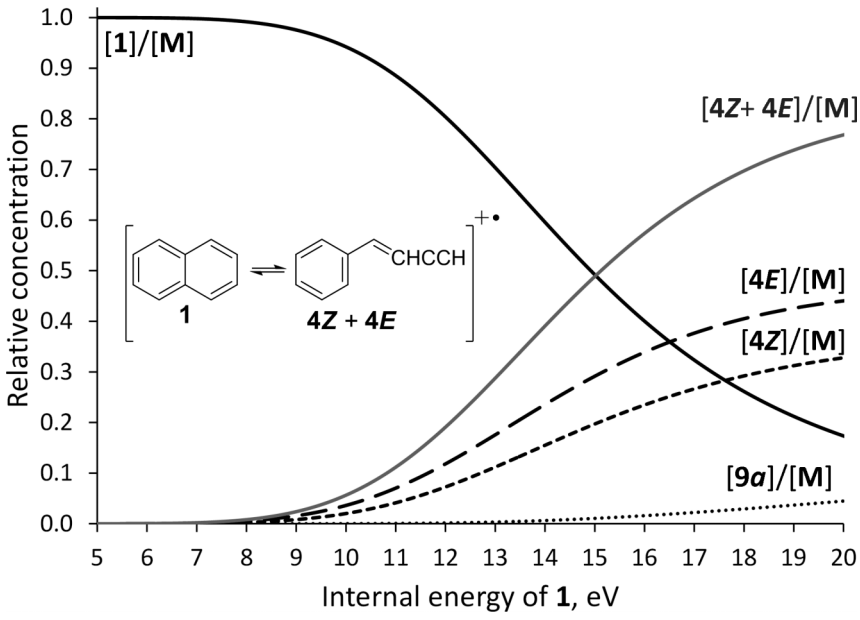

FIG. 2. The pre-equilibrium approximation applied to the isomers **1**–**9a** of the naphthalene molecular ion: relative concentrations of the isomers as a function of internal energy of the ion **1**.

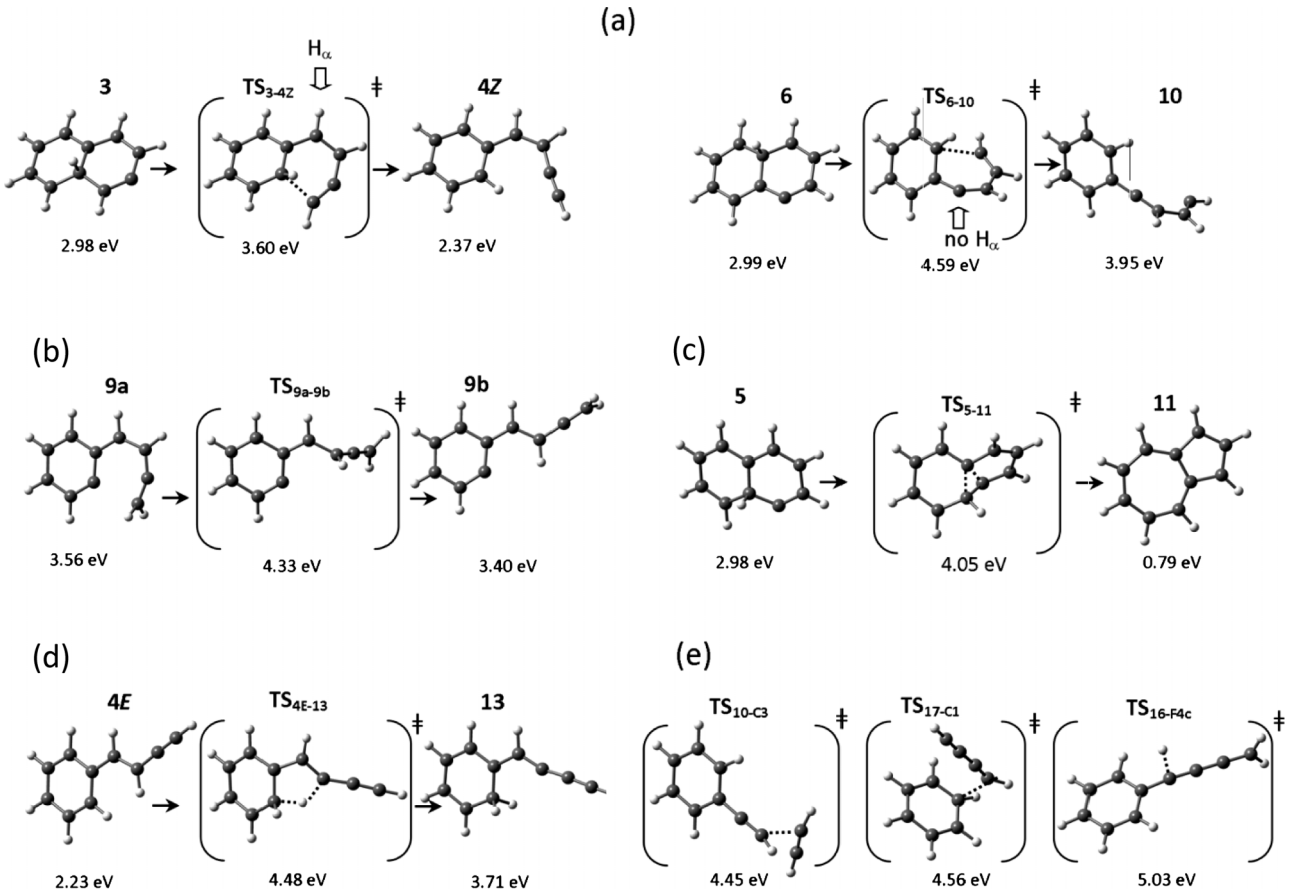

FIG. 3. UB3LYP/6-31G(d,p)-optimized geometries of selected ions $[C_{10}H_8]^{+\bullet}$ and transition structures, showing the relative UB3LYP/6-311+G(3df,2p)//UB3LYP/6-31G(d) energies of the ground states. These models are implied in steps of (a) ring opening, (b) McLafferty rearrangement, (c) *s-cis*/*s-trans* isomerization, (d) ring-expansion/ring-contraction, and (e) dissociation.

states at 5.10 and 5.09 eV) and lower k(E)'s (Figs. 1(c) and 1(d)) than the competitive processes involving ring-opened structures (e.g., **3** → **4*Z*** and **6** → **10**). Thus, $\mathbf{F}_{4a}$ and $\mathbf{F}_{4b}$ are barely formed and H$^\bullet$ loss proceeds through a different mechanism to yield ion $\mathbf{F}_{4c}$ (branch B). The hydrogen atoms of **M** are hard to remove from the two-ring fused system (through **1**,**6** → $\mathbf{F}_{4a}$, **1**,**3** → $\mathbf{F}_{4b}$, or **8** → $\mathbf{F}_{3a}$), being trapped in a multiple-minima energy surface by which they are randomized through the structures. The saturation of the central carbons, as in **3** or **6**, brings about ring openings (**3** → **4*Z*** and **6** → **10**) before C–H dissociations. Fig. 3(a) shows the molecular models of these two steps. One of the corresponding transition states, $\mathbf{TS}_{3-4Z}$, does not contribute to the decomposition of the parent ions **M**, because it has its two α-hydrogen atoms on the ring that is being destroyed, stabilizing the structure by reducing the strain and making the corresponding reaction fast enough to keep it in equilibrium in **M**. In contrast, the other one ($\mathbf{TS}_{6-10}$), with a ground-state energy 0.99 eV higher, takes the system out of the equilibrium region towards branch C. There is another ring opening in **M** generating **9*a***, a species with one of the highest ground states inside the equilibrium region **M**, because the phenyl ring has incomplete valences on one of the carbons (Fig. 3(b)). However, its formation is less energetically demanding than, for instance, that of the azulene ion (Scheme 3). The pathway to H$^\bullet$ ejection gets started here, with the *s-cis*/*s-trans* isomerization **9*a*** → **9*b*** through a transition state at 4.33 eV (Fig. 3(b)). This new conformation allows one H atom of the side chain to be transferred to the ring by a 1,4-H shift, **9*b*** → **16**, that recovers the full valences of the aromatic ring, lowering the ground state in the new species, the 1-phenyl-butatriene radical cation (**16**). According to the present work, this is the species that actually loses a hydrogen atom. In this branch, $[\mathbf{I}_B] = [\mathbf{9b}] + [\mathbf{16}]$, with **9*b*** having very close rate constants in both directions, **9*b*** → **9*a*** and **9*b*** → **16**.

H_2 loss from **8** is the most probable cleavage step, in which the energy increase due to the C–H stretching is somewhat compensated by the formation of a new H–H bond, with a transition state at 4.81 eV.

Species **10** is produced irreversibly and dissociates as soon as formed, as can be seen in Fig. 1(e), where the subsequent dissociation step, **10** → **C3**, is much faster than the reverse reaction **10** → **6**. [**10**] clearly stays at a steady state, with a slow formation and a fast decomposition, $(k_{16} + k_{-15}) \gg k_{15}$ (Fig. 1(e)). Consequently, k_{15} acts as the rate-limiting step in the C_2H_2 loss through this branch that yields the major fragment $[M–C_2H_2]^{+\bullet}$ at moderate and high energies, the phenylacetylene radical cation ($\mathbf{F}_{2b}$). This is a branch with only one intermediate; therefore, $[\mathbf{I}_C] = [\mathbf{10}]$. The remainder two decomposition steps from **M** to form C_2H_2 involve breaking or forming C–C bonds, or both. In Scheme 3, ring rearrangements can take place on **1** and **5**. On one hand, the two α-carbon atoms of the naphthalene molecular ion can directly establish a new bond to yield the bicyclic structure **7**, the

highest intermediate still in **M**. The dissociation of one C–C bond **7** → **12** connects **M** to branch D, to eventually yield the benzocyclobutadiene radical cation (**F_{2a}**), as the minor structure for $[M–C_2H_2]^{+\bullet}$. For this region of the PES profile, $[\mathbf{I}_D] = [\mathbf{12}]$. On the other hand, the lowest transition state in the energy profile that contributes to directly decompose **M** is **$TS_{5–11}$** at 4.05 eV (Fig. 3(c)). It consists in a simultaneous ring-expansion/ring-contraction that yields the azulene ion (**11**) in branch E. The reverse reaction competes with the step by which the tropylium ring forms the new bicyclic structure **14**, having identical barriers (3.26 eV). The last ion has the same fate as the bicyclic **7**, that is, two sequential C–C bond cleavages (**14** → **15** → **C4**) to yield the pentalene radical cation (**F_{2c}**), the structure that accounts for most of the $[M–C_2H_2]^{+\bullet}$ ions at low energies. The reaction **14** → **15** is slightly faster than **14** → **11**, but they are still competitive (supplementary material),[29] and the dissociation of **15** can be the dominant step (although by a small difference) in an important energy interval (Fig. 1(f)). This way, an irreversible pathway **14** → **15** → **C4** was assumed in Scheme 3, which may be the weakest assumption in this work but simplifies the rate equations. In consequence, $[\mathbf{I}_E] \approx [\mathbf{11}] + [\mathbf{14}]$, and the irreversibility assumption of the pathway from **14** to yield a steady-state [**15**] ($[\mathbf{15}] = k_{19}[\mathbf{14}]/k_{20}$) makes [**15**] disappear from the rate equations, that is, $d[\mathbf{F}_{2c}]/dt = k_{20}[\mathbf{15}] = k_{19}[\mathbf{14}]$.

A fast *cis-trans* isomerization from ion **4*Z***, a 1,4-H shift step that recalls a McLafferty rearrangement (**4*E*** → **13**, with **$TS_{4E–13}$** at 4.46 eV, Scheme 3 and Fig. 3(d)), leads the system to branch A of the PES, ending with the ejection of a diacetylene molecule. The corresponding transition state structure is shown in Fig. 3(d). The resulting species (ion **13**) suffers a 1,2-H shift on the ring (**13** → **17**, with **$TS_{13–17}$** at 4.65 eV, Scheme 3) almost as fast as the reverse reaction **13** → **4*E*** (supplementary material).[29] This pathway (**4*E*** → **13** → **17**) is much easier than the sequential 1,2-H shifts **4*Z*** → **18** → **17** of Scheme 1 (reported by Dyakov and co-workers)[13] with UB3LYP/6-311+G(3df,2p)//UB3LYP/6-31G(d) transition states at 4.52 and 4.96 eV (these species were not included in Scheme 3). The concentration of the steady state intermediate in this branch is $[\mathbf{I}_A] = [\mathbf{13}] + [\mathbf{17}]$, where, in contrast to branch C, the decomposition steps of **13** (**13** → **4*E*** and **13** → **17**) are more competitive (supplementary material).[29]

E. Fragmentation rate constants

At the end of Sec. III B, the reaction rates to yield the different fragment ions were defined in terms of the elementary steps, which have the form $d[\boldsymbol{J}]/dt = k_{\text{last}}[\boldsymbol{s}_{\mathbf{dec}}]$. In Sec. III A, the equations had been written in terms of the parent ion concentration [**M**], as $d[\boldsymbol{J}]/dt = k_J[\mathbf{M}]$, to demonstrate the validity of Eqs. (3)–(6). Now, Eqs. (3)–(6) are used to calculate the rate constants from the mechanism and the outcomes of the direct counting of vibrational states. This way, the total decay rate constant is given by $k = k_1 + k_2 + k_3 + k_4$, where k_1 governs the channel $[M–C_4H_2]^{+\bullet}$, going through the intermediate region $\mathbf{I}_A$ (case (iii), Scheme 2) and k_3 defines $[M–H_2]^{+\bullet}$, corresponding to a direct decomposition of **M** (case (i)). In turn, to account for different isomer fragment ions with the same m/z in the other two channels, k_2 ($[M–C_2H_2]^{+\bullet}$) and k_4 ($[M–H^{\bullet}]^+$) were themselves divided into the fragmentation rate constants to produce the different structures, $k_2 = k_{2a} + k_{2b} + k_{2c}$ and $k_4 = k_{4a} + k_{4b} + k_{4c}$. There are three intermediates for $[M–C_2H_2]^{+\bullet}$, $\mathbf{I}_C$ (case (ii)), $\mathbf{I}_D$ (case (ii)), and $\mathbf{I}_E$ (case (iii)), and one for $[M–H^{\bullet}]^+$ via branch B ($\mathbf{I}_B$, case (iii)). The other two terms of k_4 describe direct decompositions from **M** to **F_{4a}** and **F_{4b}** (case(i)). It should be recalled that in branch E, an additional approximation of rate-controlling steps was done to exclude [**15**] from the intermediate $\mathbf{I}_E$.

The microcanonical rate constants calculated by Eqs. (3)–(8) are plotted in Fig. 4. First, in this model the "critical energy" for every fragmentation (i.e., the barrier or threshold from which the apparent sum of states $c_J\sigma_{\text{last}}N^{\ddagger}_{\text{last}}$ start) is given by the ground-state energy ($E^{\ddagger}_{\text{gs},i}$) of the highest transition state along the pathway (e.g., **$TS_{13–17}$** for k_1). For isomeric fragment ions (e.g., **F_{4a}**, **F_{4b}**, and **F_{4c}**), there are

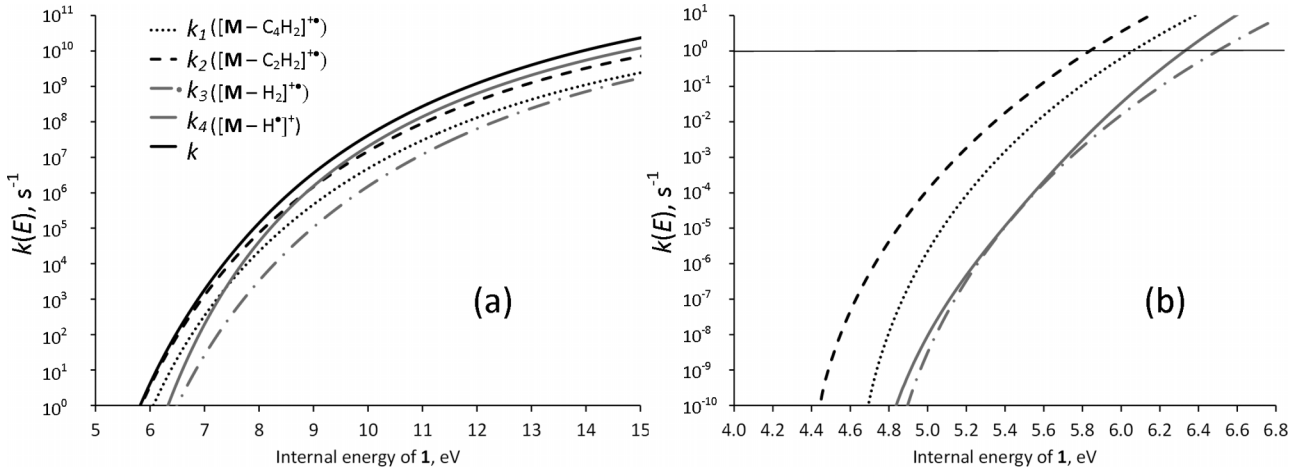

FIG. 4. Microcanonical rate constants as a function of internal energy of the molecular ion **1** for the total decay of **M**(k) discriminated into the four fragmentation channels (k_1, k_2, k_3, and k_4), calculated by Eqs. (3)–(8). (a) and (b) show different intervals of the k_J's. The following values σ of were used. $\sigma_i = 8$ for **$TS_{12–C2}$**, **$TS_{7–12}$**, **$TS_{10–C3}$**, **$TS_{6–10}$**, **$TS_{5–11}$**, **$TS_{14–15}$**, **$TS_{5–9}$**, **$TS_{9–14}$**, **$TS_{6–F4a}$**, and **$TS_{3–4b}$**; $\sigma_i = 4$ for **$TS_{1–F4a}$**, **$TS_{1–4b}$**, and **$TS_{8–F3a}$**; $\sigma_i = 2$ for **$TS_{9a–9b}$** and **$TS_{9b–16}$**; and $\sigma_i = 1$ for the rest.

different "highest" transition states (e.g., $\mathbf{TS_{1–F4a}}$, $\mathbf{TS_{1–F4b}}$, and $\mathbf{TS_{16–F4c}}$), but the one defining the critical energy of the channel as a whole is that of minimum energy (e.g., $\mathbf{TS_{1–F4a}}$). This way, $\mathbf{TS_{13–17}}$, $\mathbf{TS_{14–15}}$, $\mathbf{TS_{8–F3a}}$, and $\mathbf{TS_{1–F4a}}$ define the critical energies of the global fragmentations, yielding the following values, namely, 4.65 eV for $[M–C_4H_2]^{+\bullet}$, 4.43 eV for $[M–C_2H_2]^{+\bullet}$, 4.81 eV for $[M–H_2]^{+\bullet}$, and 4.75 eV for $[M–H^\bullet]^+$. However, these values are just a consequence of the structures included in the model, but they do not necessarily have an important effect on the k(E)'s in a detectable time window. For instance, the critical energy of channel k_4 is given by $\mathbf{TS_{1–F4a}}$ as 4.75 eV, but if this transition state had not been considered in the modeling, the barrier would have been 4.83 eV (corresponding to $\mathbf{TS_{1–F4b}}$), or even 5.03 eV ($\mathbf{TS_{16–F4c}}$) if the direct dissociation of **1** had not been included at all. That is, the model could work approximately in the same way, even if one minor fragmentation pathway, such as k_{4a} or k_{4b}, is removed from the rate equations. This is because nothing really detectable is happening at such low energies (~4–5 eV, Fig. 4(b)). Fig. 4 shows that even at 5.82 eV, the total decay rate constant is just 1 s^{-1}, meaning that the species are decomposing too slowly to be detected (with half-lives of ca. 1 s). A more convenient energetic parameter to characterize the fragmentations would be the energy at which the channel J takes on some defined value of the rate constant. As an example, if by convention this value were fixed as $k_J = 1\ s^{-1}$, then the threshold energies for the channels would be 6.06 eV for $[M–C_4H_2]^{+\bullet}$, 5.84 eV for $[M–C_2H_2]^{+\bullet}$, 6.50 eV for $[M–H_2]^{+\bullet}$, and 6.33 eV for $[M–H^\bullet]^+$, which describe the rate constants of Fig. 4(a) much better than the critical energies.

According to Fig. 4(a), k_2 dominates at energies <8.91 eV, with k_1 being the second channel up to <7.39 eV. However, although k_4 has a higher critical energy, it also exhibits a

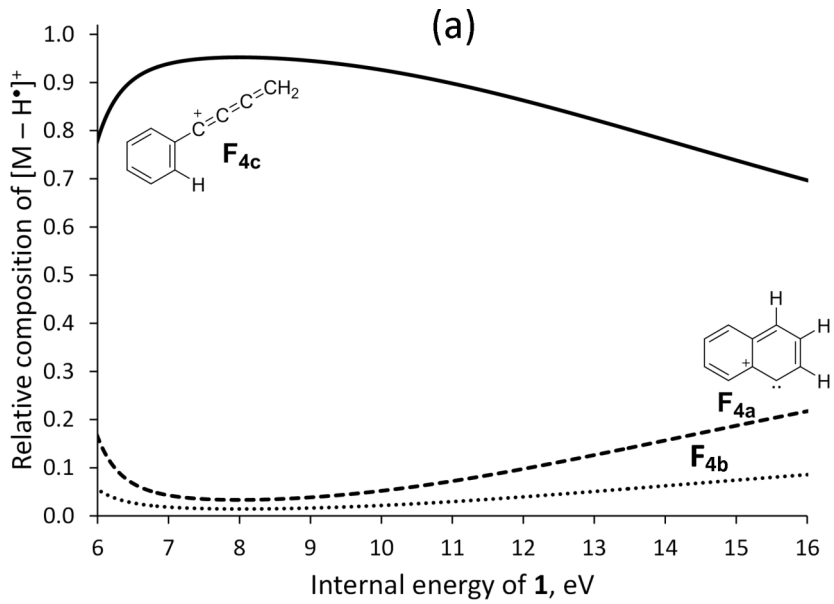

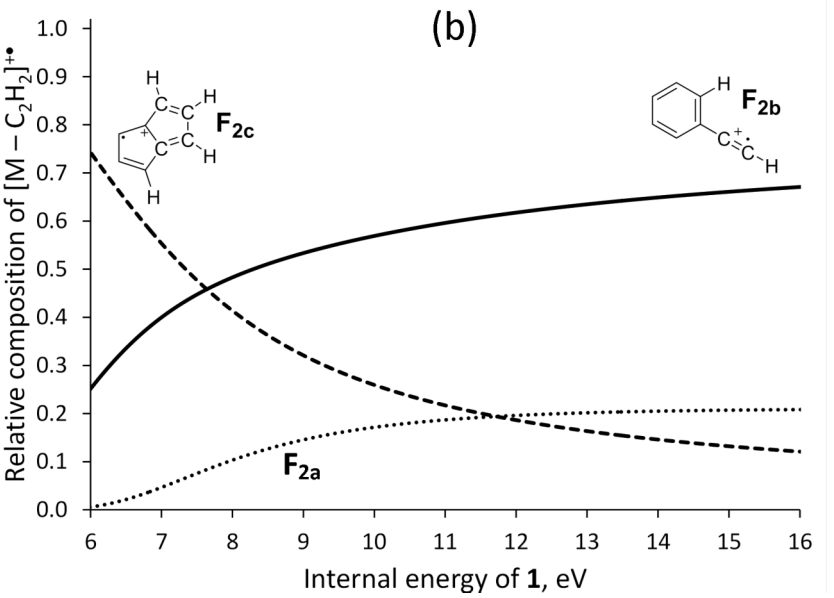

FIG. 5. Relative composition of the fragment ions (a) $[M–H^\bullet]^+$ and (b) $[M–C_2H_2]^{+\bullet}$, according to Eq. (23).

more pronounced slope, which makes k_4 overcome k_1 at 7.39 eV, and k_2 at 8.91 eV. The higher slope of k_4 is probably due to the vibrational nature of the transition states of the first steps towards the branches: $\mathbf{TS}_{4E-13}$, $\mathbf{TS}_{9a-9b}$, and $\mathbf{TS}_{6-10}$ (Figs. 3(b)-3(d)). $\mathbf{TS}_{9a-9b}$ has lower frequencies (data not shown) that imply a higher sums-of-states. In other words, $\mathbf{TS}_{4E-13}$ and $\mathbf{TS}_{6-10}$ are "tighter" transition states. These effects are incorporated in k_1, k_{2b}, and k_{4c} through the corresponding energy-dependent coefficients c_1, c_{2b}, and c_{4c} (Eqs. (5) and (6)). The explicit form of all the rate constants is shown in the supplementary material.[29] k_3 is the slowest channel through the entire energy range.

Finally, the ratio given in Eq. (23) was used to establish how much of every isomeric fragment ion is being formed in this model,

$$\frac{[J_n]}{[J]} = \frac{k_{J,n}}{k_J}, \tag{23}$$

where

$$k_J = \sum_n k_{J,n} \tag{24}$$

and

$$[J] = \sum_n [J_n]\,. \tag{25}$$

Equations (23)–(25) mean that $[\mathbf{F_{2a}}]/[\mathbf{M} - C_2H_2]^{+\bullet} = k_{2a}/k_2$, $[\mathbf{F_{2b}}]/[\mathbf{M} - C_2H_2]^{+\bullet} = k_{2b}/k_2$, and $[\mathbf{F_{2c}}]/[\mathbf{M} - C_2H_2]^{+\bullet} = k_{2c}/k_2$, where $k_2 = k_{2a} + k_{2b} + k_{2c}$. Similar expressions can be written for the $H^\bullet$ loss, using $\mathbf{F_{4a}}$, $\mathbf{F_{4b}}$, and $\mathbf{F_{4c}}$. These are plotted in Fig. 5 as a function of energy, starting at 6 eV. According to Fig. 5(a), $\mathbf{F_{4c}}$ is the major $[M–H^\bullet]^+$ structure, accounting for ≥70% of the fragmentation in the energy range shown. In the important interval 7–11 eV, $\mathbf{F_{4c}}$ constitutes ≥95% and $\mathbf{F_{4a}}$ constitutes ≤7%. This result is contrary to the conventional wisdom about the $H^\bullet$ loss in the mass spectra of naphthalene, and it could have consequences on the way other polycyclic aromatic hydrocarbon compounds are seen. In turn, $[M–C_2H_2]^{+\bullet}$ is a mixture of the three isomeric structures, with the pentalene radical cation ($\mathbf{F_{2c}}$) as the predominant species at low energies, up to 7.63 eV, above which the phenylacetylene ion ($\mathbf{F_{2b}}$) becomes the most abundant structure. According the present model, the benzocyclobutadiene ion ($\mathbf{F_{2b}}$) is a minor component of the fragment ion $[M–C_2H_2]^{+\bullet}$.

F. Comparison with the experiment

This kinetic scheme was tested against the experimental iPEPICO mass spectra of naphthalene by using Eqs. (11) and (12). The results shown in Fig. 6 are reasonably good, with coefficients of determination R^2 of 0.932 for the parent ion curve, and 0.833, 0.985, 0.623, and 0.860 for $[M–C_4H_2]^{+\bullet}$, $[M–C_2H_2]^{+\bullet}$, $[M–H_2]^{+\bullet}$, and $[M–H^\bullet]^+$, respectively. In general, both the experiment and modeling show the same trend, the most abundant processes are $[M–H^\bullet]^+$ and $[M–C_2H_2]^{+\bullet}$, with $[M–H_2]^{+\bullet}$ as the minor fragmentation. This suggests that the portion of Fig. 4(a) relevant for this experiment starts at 7.39 eV, where $k_4 \geq k_1$. In correspondence with Fig. 4(a), where there is an interval (under 8.91 eV) for which $k_2 > k_4$ and after which $k_2 < k_4$, the breakdown graph exhibits a middle-energy region with $[M–C_2H_2]^{+\bullet} > [M–H^\bullet]^+$, but at higher energies, $[M–C_2H_2]^{+\bullet} < [M–H^\bullet]^+$. The model yields the right shapes for all the curves. The best description is that for $[M–C_2H_2]^{+\bullet}$, the channel with the highest "mechanistic" diversity, in the sense that three very different pathways are mixed together, with structures clearly distinguishable for two energy regimes.

The total parent ion decay and the $H^\bullet$ loss are underestimated towards the low-energy region. Four possible causes are (i) the existence of important pathways for this fragmentation not found in this work, (ii) the overestimation of the energy barriers by the DFT method used here, (iii) the tunneling of the barriers by the hydrogen atom, and (iv) the

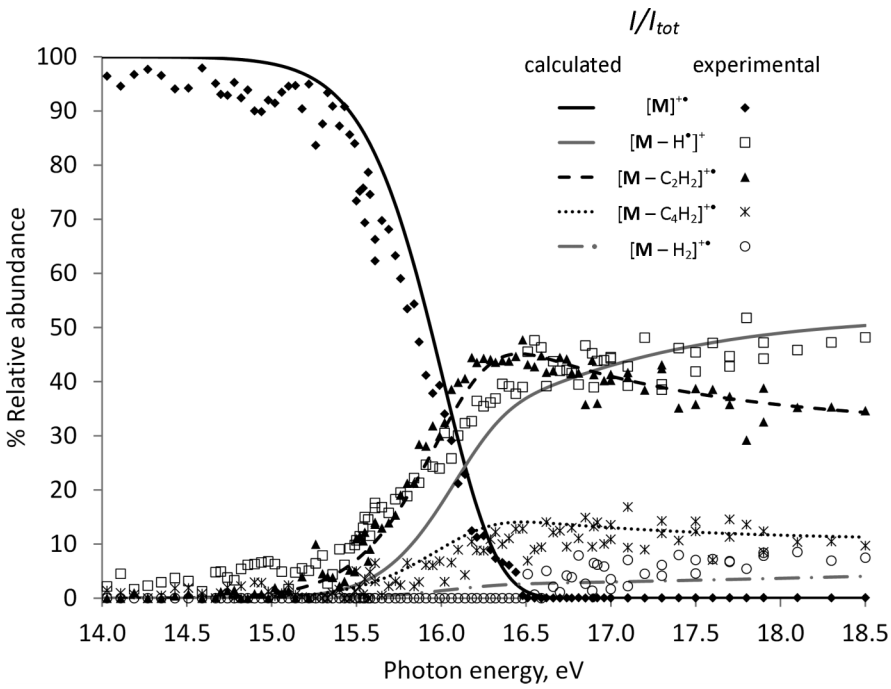

FIG. 6. iPEPICO breakdown graph for the naphthalene radical cation over the photon energy range of 14.0-20.5 eV (Ref. 11) compared to the theoretical curves calculated by Eqs. (11) and (12), using $k = k_1 + k_2 + k_3 + k_4$ of Fig. 4.

shape of the energy distribution function. In the first case, some possible additional mechanisms can be explored in the future, especially in a region relevant at low energies, such as branch E. If the problem is about the electronic calculations overestimating barriers, and a better level of theory is used, it is possible that the fragment ion $\mathbf{F_{4a}}$ accounts for more of the $[M–H^{\bullet}]^+$ ion at low energies. To deal with quantum penetration of barriers, tunneling probabilities can be included in the sums of states to improve the description.[9] A tunneling explanation is reasonable given that the theoretical PES can be fitted to the experimental data by adjusting the $H^{\bullet}$ loss channel barrier by only ca. 50 meV. Finally, two suggestions to improve the function $p_M(E, h\nu)$ (Eq. (9)) are (i) using the density of states of the parent ions ρ_M (Eq. (22)) instead of that of the molecule, and (ii) including the possibility of some thermal-like redistribution of energy by allowing for some change in temperature. However, all these tasks are beyond of the scope of the current work.

G. A more general look at the kinetic treatment

In general, the rate constant of a given channel is a superposition of k's, such as $k_2 = k_{2a} + k_{2b} + k_{2c}$, in which each k is the product of a coefficient c_J by a term of the form $\sigma_{\text{last}} N^{\ddagger}_{\text{last}} / (h\rho_M)$ (Eq. (3)). According to the definition of c_J given in Eqs. (4)–(6), this quantity ranges from 0 to 1.

To check the behavior of the c_J's, they were plotted in Fig. 7. c_{2b} is too low ($\sim 10^{-3}$) to be visualized in this picture, and c_1 is less than 0.05. Consequently, these processes are controlled by the formation of **10** and **13**, respectively, with faster dissociations of the intermediates $\mathbf{I_C}$ and $\mathbf{I_A}$. In turn, c_{2a}, c_{2c}, and c_{4c} are decreasing functions of energy with different slopes, indicating a change of behavior with energy. c_{2a} and c_{4c} are switching the reaction from a process controlled by the dissociation step at low energies ($c_J = 1$) to one controlled by the formation of the intermediate at higher energies. For instance, the fragmentation to $\mathbf{F_{2a}}$ can be seen as a reaction being displaced from $k_{2a} = \sigma_{14} N^{\ddagger}_{12-C2} / (h\rho_M)$ to $k_{2a} \approx \sigma_{12} N^{\ddagger}_{7-12} / (h\rho_M)$. On the other hand, c_{2c} is coming down from 1 at low energies, but it takes on some middle values at high energies (e.g., c_{2c} is 0.50 at 12.17 eV), suggesting that the steps **11** → **5** and **14** → **15** are more competitive.

To generalize, c_J acts as a correction coefficient on a "zeroth-order" dissociation rate constant $k_J^{(0)} = \sigma_{\text{last}} N^{\ddagger}_{\text{last}} / (h\rho_M)$, so the total decay can be characterized by

$$k = \sum_J c_J k_J^{(0)}, \tag{26}$$

$$k_J^{(0)} = \frac{\sigma_{\text{last}} N^{\ddagger}_{\text{last}}}{h\rho_M}. \tag{27}$$

An alternative interpretation is that, given that the fragmentation occurs, c_J acts as the probability that the system reacts with a rate constant $k_J^{(0)}$. $N^{\ddagger}_{\text{last}}$ describes a dissociative transition state that usually has lower vibrational frequency values than the original molecular ion, and ρ_M describes the parent ion that can be a mixture of equilibrated isomers or a pure ion ($\rho_M \approx \rho_1$ in an important energy range). This implies that when isomerization is not significant, $k_J^{(0)} \approx \sigma_{\text{last}} N^{\ddagger}_{\text{last}} / (h\rho_1)$ is a good approximation.

These ideas can be extended over other systems, when they are reasonably described by Scheme 2(a), that is, one parent ion that can adopt different structures at equilibrium, and undergoes fragmentation directly or through steady-state intermediates. However, a detailed knowledge of the mechanism seems impracticable in most cases; therefore, some approximations are usually made, such as that in which the frequencies of the molecular ion are calculated at some level of theory and used to estimate the density of states of the parent ion and the sum of states of the transition state. For the latter, one frequency is removed from the parent ion and few modes (with low frequencies) are scaled by a factor.[27] Since the dissociative transition states of Fig. 3(e) have lower frequencies than the naphthalene molecular ion, scaling down the frequencies of the molecular ion in a

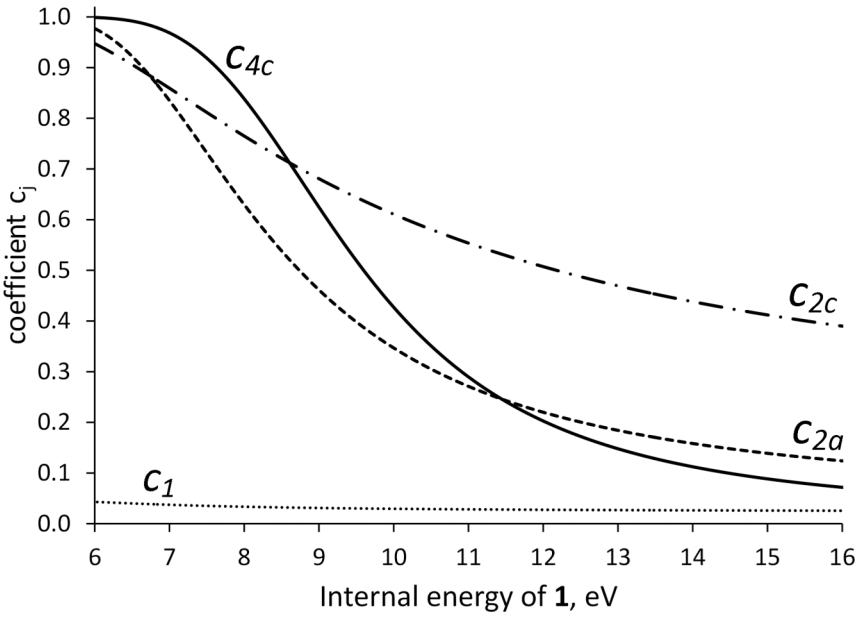

FIG. 7. Energy-dependent coefficients c_j, calculated by Eqs. (4)–(6).

hypothetical transition state seems a reasonable approximation for the fragmentation of **M** through the branches in Scheme 3. In another approach recently published for the iPEPICO of quinoline and isoquinoline, one transition state on the PES, considered as rate-limiting, is used to calculate the sum of states of the rate constant.[28] In both cases (scaling down the parent ion frequencies or calculating one first-order saddle point on the PES), the use of only one transition-state sum-of-states could in principle be equivalent to the calculation of some $k_J^{(0)} \approx \sigma_{\text{last}} N_{\text{last}}^{\ddagger} / (h\rho_1)$. This "single transition state" approximation may be subject to a further treatment such as mixing isomeric structures in the parent ion to improve ρ_M, which decreases the rate constant. Second, mixing different transition states $N_{\text{last}}^{\ddagger}$ for the same channel as linear combinations of $k_J^{(0)}$'s to mimic reactions happening through different mechanisms or yielding different structures (as in branches C–E). And third, coming up with some approximated method to estimate the coefficients c_J.

IV. CONCLUSION

With the exception of the H_2 loss (that can be rationalized in terms of the structure of the molecular ion), the mass spectrum of naphthalene exhibits characteristics attributable to chemically different species. It behaves like the **4Z**/**4E** ions to eliminate diacetylene and like the 1-phenyl-butatriene ion to lose a hydrogen atom. To eliminate an acetylene molecule at low energies, it looks like the azulene ion, but at high energies is more similar to **4Z**/**4E**. However, probably none of these isomers are significantly present in the ionized gas phase. Conversely, when naphthalene is given enough energy during the ionization (or the molecular ion is somewhat activated), these isomeric structures are formed at steady states, which constitute "open gates" to the different fragmentations. These species are connected through a common potential energy surface. They are all part of the same reactive system. That does not mean that their mass spectra should look identical, because they have different ground-state energies and vibrational frequencies, which implies unequal energetic requirements. The chemistry of the naphthalene molecular ion is then a superposition of the chemistry of different species. To account for such as diversity, the fragmentation rate constants should be calculated as the superposition of at least two transition states, one for an isomerization and the other for a dissociation. The linear combination of different pathways within the same channel further improves the kinetic description of the mass spectrum.

ACKNOWLEDGMENTS

P.M.M. thanks the Natural Sciences and Engineering Research Council of Canada for continuing financial support. E.S. thanks the *Departamento Administrativo de Ciencia, Tecnología e Innovación* (*Colciencias*), Colombia and *Colfuturo* for the financial support through the *Programa de Doctorados en el Exterior 2012*.

[1]C. Jia and S. Batterman, Int. J. Environ. Res. Public Health **7**, 2903 (2010).
[2]M. Frenklach, Phys. Chem. Chem. Phys. **4**, 2028 (2002).
[3]J. Filley and J. T. McKinnon, Combust. Flame **124**, 721 (2001).
[4]A. Goldaniga, T. Faravelli, and E. Ranzi, Combust. Flame **122**, 350 (2000).
[5]M. Kapuci, Z. Ulker, S. Gurkan, and L. Alpsoy, Toxicol. Ind. Health **30**, 82 (2014).
[6]P.-h. Li, S.-f. Kong, C.-m. Geng, B. Han, B. Lu, R.-f. Sun, R.-j. Zhao, and Z.-p. Bai, Environ. Sci.: Processes Impacts **15**, 623 (2013).
[7]G. A. George and G. C. Morris, J. Mol. Spectrosc. **26**, 67 (1968).
[8]J. Niu, P. Sun, and K.-W. Schramm, J. Photochem. Photobiol., A **186**, 93 (2007).
[9]B. Sztáray, A. Bodi, and T. Baer, J. Mass Spectrom. **45**, 1233 (2010).
[10]Y. Gotkis, M. Oleinikova, M. Naor, and C. Lifshitz, J. Phys. Chem. **97**, 12282 (1993).
[11]Y.-P. Ho, J. R. C. Dunbar, and C. Lifshitz, J. Am. Chem. Soc. **117**, 6504 (1995).
[12]B. West, C. Joblin, V. Blanchet, A. Bodi, B. Sztáray, and P. M. Mayer, J. Phys. Chem. A **116**, 10999 (2012).
[13]Y. A. Dyakov, C.-K. Ni, S. H. Lin, Y. T. Lee, and A. M. Mebel, Phys. Chem. Chem. Phys. **8**, 1404 (2006).
[14]H. W. Jochims, H. Rasekh, E. Rühl, H. Baumgärtel, and S. Leach, Chem. Phys. **168**, 159 (1992).
[15]K. Schroeter, D. Schröder, and H. Schwarz, J. Phys. Chem. A **103**, 4174 (1999).
[16]M. J. Frisch, G. W. Trucks, H. B. Schlegel, G. E. Scuseria, M. A. Robb, J. R. Cheeseman, G. Scalmani, V. Barone, B. Mennucci, G. A. Petersson, H. Nakatsuji, M. Caricato, X. Li, H. P. Hratchian, A. F. Izmaylov, J. Bloino, G. Zheng, J. L. Sonnenberg, M. Hada, M. Ehara, K. Toyota, R. Fukuda, J. Hasegawa, M. Ishida, T. Nakajima, Y. Honda, O. Kitao, H. Nakai, T. Vreven, J. A. Montgomery, Jr., J. E. Peralta, F. Ogliaro, M. Bearpark, J. J. Heyd, E. Brothers, K. N. Kudin, V. N. Staroverov, R. Kobayashi, J. Normand, K. Raghavachari, A. Rendell, J. C. Burant, S. S. Iyengar, J. Tomasi, M. Cossi, N. Rega, J. M. Millam, M. Klene, J. E. Knox, J. B. Cross, V. Bakken, C. Adamo, J. Jaramillo, R. Gomperts, R. E. Stratmann, O. Yazyev, A. J. Austin, R. Cammi, C. Pomelli, J. W. Ochterski, R. L. Martin, K. Morokuma, V. G. Zakrzewski, G. A. Voth, P. Salvador, J. J. Dannenberg, S. Dapprich, A. D. Daniels, O. Farkas, J. B. Foresman, J. V. Ortiz, J. Cioslowski, and D. J. Fox, GAUSSIAN 09, Revision A.02, Gaussian, Inc., Wallingford, CT, 2009.
[17]K. Fukuy, J. Phys. Chem. **74**, 4161 (1970).
[18]P. A. Scott and L. Radom, J. Phys. Chem. **100**, 16502 (1996).
[19]T. Beyer and D. F. Swinehart, Commun. ACM **16**, 379 (1973).
[20]T. Baer and W. L. Hase, *Unimolecular Reaction Dynamics: Theory and Experiments* (Oxford, New York, 1996), pp. 9, 26-31, 131-134, 183-184, 206, 212–281.
[21]T. Baer and P. Mayer, J. Am. Soc. Mass Spectrom. **8**, 103 (1997).
[22]F. G. Helfferich, "Kinetics of multistep reactions," in *Comprehensive Chemical Kinetics*, edited by N. J. B. Green (Elsevier B.V, Amsterdam, 2004), Vol. 8, pp. 77–93.
[23]See http://www.wolfram.com for MATHEMATICA, Wolfram Research, Inc., Champaign, IL.
[24]M. C. R. Cockett, H. Ozeki, K. Okuyama, and K. Kimura, J. Chem. Phys. **98**, 7763 (1993).
[25]V. Gabelica and E. D. Pauw, Mass Spectrom. Rev. **24**, 566 (2005).
[26]L. Drahos, R. M. A. Heeren, C. Collette, E. D. Pauw, and K. Vékey, J. Mass Spectrom. **34**, 1373 (1999).
[27]B. West, A. Sit, S. Mohamed, C. Joblin, V. Blanchet, A. Bodi, and P. M. Mayer, J. Phys. Chem. A **118**, 9870 (2014).
[28]J. Bouwman, B. Sztáray, J. Oomens, P. Hemberger, and A. Bodi, J. Phys. Chem. A **119**, 1127 (2015).
[29]See supplementary material at http://dx.doi.org/10.1063/1.4930000 for the general ideas for Python coding of the density-of-states counting, additional RRKM rate constants for the steps in Scheme 3 (Fig. S1), explicit forms of the rate constants of Fig. 4, and a comparison of one of the unimolecular reactions treated with and without a hindered internal rotor (Fig. S2).